This article has been accepted for publication in a future issue of this journal, but has not been fully edited. Content may change prior to final publication. Citation information: DOI 10.1109/MDAT.2014.2336211, IEEE Design and Test

A Case Study of Signal-to-Noise Ratio in Ring-Based Optical Networks-on-Chip

Luan H.K. Duong, *Student Member, IEEE*, Mahdi Nikdast, *Member, IEEE*, Sebastien Le Beux, *Member, IEEE*, Jiang Xu, *Member, IEEE*, Xiaowen Wu, *Student Member, IEEE*, Zhehui Wang, *Student Member, IEEE*, Peng Yang

***Abstract*—Microresonators have been utilized to construct optical interconnection networks. One of the drawbacks of these microresonators is that they suffer from intrinsic crosstalk noise and power loss, resulting in Signal-to-Noise Ratio (SNR) reduc-tion and system performance degradation at the network level. The novel contribution of this paper is to systematically study the worst-case crosstalk noise and SNR in a ring-based ONoC, the Corona. In the paper, Corona's data channel and broadcast bus are investigated, with formal general analytical models presented at the device and network levels. Leveraging our detailed analytical models, we present quantitative simulations of the worst-case power loss, crosstalk noise, and SNR in Corona. Moreover, we compare the worst-case results in Corona with those in mesh-based and folded-torus-based ONoCs, all of which consist of the same number of cores as Corona. The quantitative results demonstrate the damaging impact of crosstalk noise and power loss in Corona: the worst-case SNR is roughly 14.0 dB in the network, while the worst-case power loss is substantially high at -69.3 dB in the data channel.**

***Keywords*—Optical networks-on-chip, Corona ring-based ONoC, crosstalk noise, signal-to-noise ratio.**

I. Introduction

WITH the increasingly urgent need for higher speed and more powerful computational performance, integrating a large number of cores on a single die has been mainstream for the last few decades. To support these multi-core sys-tems, different networks-on-chip (NoCs) structures have been proposed to replace traditional interconnection networks [1]. However, as the number of processing cores on a single die continues to increase, the metallic interconnects in NoCs seem to be falling behind the high-bandwidth and low-latency requirements. This issue has been addressed by the proposed Optical Networks-on-Chip (ONoCs) for ultra-high bandwidth and low-power energy consuming interconnection networks.

Among the proposed ONoCs interconnect structures, ring-based ONoCs [2], [3], have been introduced due to their advantages of supporting on-chip bandwidth with on-chip optical crossbars. Different from off-chip bandwidth, on-chip bandwidth is not limited by the number of package pins, which is forecast not to considerably increase [4]. Moreover, on-chip crossbars improve network latency with electrical-optical/optical-electrical converters implemented at the end of the ring [2], [4].

Luan H.K. Duong, Mahdi Nikdast, Jiang Xu, Xiaowen Wu, Zhehui Wang, and Peng Yang are with the Department of Electronic and Computer Engineering, Hong Kong University of Science and Technology, Hong Kong.

Sebastien´ Le Beux is with Lyon Institute of Nanotechnology, Ecole Centrale de Lyon, France.

Email: hklduong@ust.hk, mnikdast@connect.ust.hk, jiang.xu@ust.hk, sebastien.le-beux@ec-lyon.fr

This project is supported by Huawei Technologies Co., Ltd.

Additionally, Dense Wavelength-Division Multiplexing (DWDM) is inevitable in the future ONoCs [2]. In DWDM, a large number of wavelengths are intergrated to provide ultra-high bandwidth for the network. Nevertheless, one of the major drawbacks of DWDM-based networks is that crosstalk noise is generated and intensified by communications among the components in the network. Regarding this issue, although crosstalk noise due to devices' imperfections might be considered negligible at the device level, crosstalk noise has severe impacts in large-scale ONoCs at the network level. This was demonstrated in [5] for single-wavelength ONoCs. In large scale ONoCs, crosstalk noise accumulates and causes power fluctuations at the receivers, restricting the network scaling. Consequently, the crosstalk noise issue should be more critical in DWDM-networks.

In this paper, for the first time, we study the crosstalk noise in a DWDM ring-based ONoC. At the device level, we carefully developed the analytical models based on the optical devices' characteristics reported in fabricated device papers. From those models, we follow a mathematical bottom-up approach to analyze the network components. With this approach, all the analytical models at the network level can be translated into the initial device level models for verification. As one of the first ring-based DWDM ONoCs, the Corona is chosen to be evaluated. Moreover, utilizing the on-chip optical crossbar, 64 clusters in Corona can independently transmit, resulting in an ultra-high bandwidth [2]. However, in the ring-based structure, crosstalk noise may accumulate from the first to the last cluster of the open ring.

The Corona ring-based ONoC is a 64 four-core clusters network. Its interconnection is formed by three different structures: the optical crossbar (data channel), the broadcast bus and the control arbitration. In our study, we focus on the data channel and the broadcast bus. Regarding the existing analytical method in [5], the basic device level's models can be used in any single-wavelength network topology. However, we model the basic optical elements in a DWDM network, which has not been introduced. We also provide analysis up to second-order crosstalk, which is a deeper level compared to [5]. At the network level, the analyses in [5] can only be applied to mesh-based and folded-torus-based ONoCs. In this paper, we utilize our proposed analytical models for Ring-based ONoCs using DWDM. Finally, we compare our results of Corona's data channel with those of the aforementioned two ONoCs. In our study, only incoherent crosstalk is considered.

The rest of the paper is organized as follows: Section II summarizes the state-of-the-art of previous works on the crosstalk

This article has been accepted for publication in a future issue of this journal, but has not been fully edited. Content may change prior to final publication. Citation information: DOI 10.1109/MDAT.2014.2336211, IEEE Design and Test

noise issue. Section III describes the basic optical elements in a general ring-based ONoC, followed by Section IV analyzing different elementary structures of Corona. Section V details the analysis of Corona's data channel and broadcast bus. Results and discussion are provided in Section VI. Section VII draws a conclusion to this paper.

II. Summary of Related Works

The crosstalk issue has been investigated in several works at both the device level and network level. On the one hand, at the device level, the amount of crosstalk seems to be negligible. For example, [6] reported an insertion loss and a crosstalk noise value of -0.2dB and -47.6dB respectively through a waveguide crossing composed of three cascaded multimode structures. At the network level, on the other hand, crosstalk noise has been noticed due to its negative impact on the SNR. In [5], Nikdast et al. analyzed the crosstalk noise and SNR in folded-torus-based ONoCs and reported that the crosstalk noise power exceeded signal power when the network size was equal to or larger than 8×8. [5] also summarized the findings of crosstalk and SNR in mesh-based ONoCs using two different routers: the optimized-optical crossbar and Crux.

Nonetheless, the aforementioned works focused on single-wavelength ONoCs, where contributed crosstalk originates from only one wavelength. Considering DWDM-based networks, several efforts have been made to analyze the effect of different wavelengths on a given wavelength. Q. Xu et al. [7] presented a four-cascaded MR-based structure and reported an extinction ratio of 13dB, with negligible crosstalk. In [8], S. Xiao et al. measured losses in a multi-wavelength micro-ring based structure.

III. Basic Optical Elements Analysis

DWDM-ONoCs are constructed by a set of basic optical elements that direct light from a source processor toward other destination processors. These elements can also be receivers, detecting and converting light back into electrical signals. In a ring-based ONoC, modulators, injectors, photo-detectors and splitters are utilized to perform the aforementioned tasks. Particularly, modulators are used to modulate the light, while detectors are placed at the end of any communication path to detect the modulated light. Splitters are exploited to distribute power by diverting a fixed portion of the optical power from one waveguide to another waveguide. Additionally, splitters can be used to split the power into equal portions. Fig. 1 shows the basic optical elements of a DWDM-based ONoC.

In Fig. 1, (a) and (b) represent a modulator's INACTIVE and ACTIVE states respectively. Meanwhile, (c) and (d) are photo-detectors in the PASSING and DETECTING states. Two kinds of splitters, which often appear in DWDM networks, are respectively modeled in (e) and (f): 1×2 and 1×4 splitters. In the following subsections, we further detail our model analysis. To facilitate our study, we provide notations for the utilized parameters in our analytical equations in Table I. The values for those parameters are from recent device fabrication results. Several parameters, such as the MR's quality factor (Q-factor) and Free-Spectral Range, are extracted from papers regarding the fabrication of Corona.

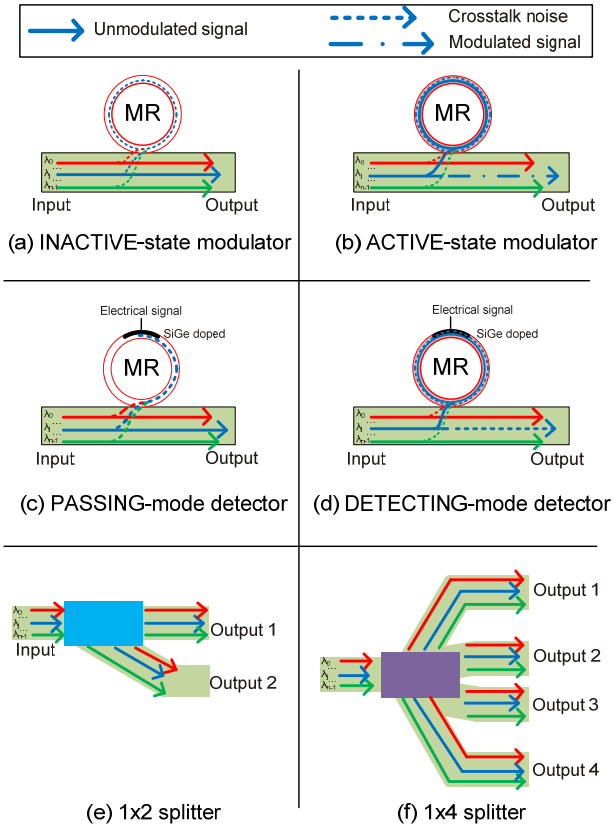

Fig. 1. Basic optical elements

TABLE I – Utilized Parameters Table

Parameter	Sym.	Value
Propagation loss	L_p	-0.274dB/cm [9]
Bending loss	L_b	-0.005dB/90° [10]
Power loss: INACTIVE modulator	L_{m_0}	-0.005dB [10]
Power loss: ACTIVE modulator	L_{m_1}	-0.6dB [10]
Power loss: PASSING detector	L_{d_0}	-0.005dB [10]
Power loss: DETECTING detector	L_{d_1}	-1.6dB [10]
Power loss: 1x2 splitter	$L_{s_{12}}$	-0.2dB [11]
Power loss: 1x4 splitter	$L_{s_{14}}$	-0.2dB [11]
Crosstalk coefficient: INACTIVE modulator	X_{m_0}	-0.001dB [10]
Crosstalk coefficient: ACTIVE modulator	X_{m_1}	-16dB [12]
Crosstalk coefficient: PASSING detector	X_{d_0}	-0.001dB [10]
Crosstalk coefficient: DETECTING detector	X_{d_1}	-16dB [12]
Q-factor	Q	9000 [4]
Free-Spectral Range	FSR	62nm [7]

This article has been accepted for publication in a future issue of this journal, but has not been fully edited. Content may change prior to final publication. Citation information: DOI 10.1109/MDAT.2014.2336211, IEEE Design and Test

A. Modulators and Detectors

Modulators and detectors are constructed by a microresonators (MR) which is coupled to a single waveguide. The MR follows a Lorentzian power transfer function peaked at its resonant wavelength λ_{MR}. For an optical signal having wavelength λ_i, the drop-port power transfer can be expressed as (1a) [8].

In (1a), κ_e^2 and κ_d^2 are respectively the fraction of optical power that the input and the drop waveguide coupled into or out of the MR, while κ_p^2 is the fraction of the intrinsic power losses per round-trip in the MR. Indeed, for a normal MR, $\kappa_e^2 \approx \kappa_d^2$ and $\kappa_p^2 = \kappa_e^2$, so the first term $\frac{2\kappa_e\kappa_d}{\kappa_e^2+\kappa_d^2+\kappa_p^2}$ approximates to one. Hence, (1a) can be written as (1b). In (1b), the -3dB bandwidth of 2δ is expressed as (1c), where Q is the Q-factor of a particular MR.

$$\frac{P_{drop}}{P_{in}} = \left(\frac{2\kappa_e\kappa_d}{\kappa_e^2+\kappa_d^2+\kappa_p^2}\right)^2\left(\frac{\delta^2}{(\lambda_i-\lambda_{MR})^2+\delta^2}\right) \quad (1a)$$

$$\frac{P_{drop}}{P_{in}} = \left(\frac{\delta^2}{(\lambda_i-\lambda_{MR})^2+\delta^2}\right) \quad (1b)$$

$$2\delta = \frac{\lambda_j}{Q}. \quad (1c)$$

The Free-Spectral Range (FSR) of a signal is also taken into account in (1b) through the difference between the MR's resonant wavelength λ_{MR} and the examined signal wavelength λ_i. Taking the two wavelengths λ_i and λ_j for example, we have $\Delta(i,j) = \lambda_i - \lambda_j = (i-j)\left(\frac{FSR}{n}\right)$, where we assume equal spacing between two consecutive wavelengths and n is the total number of wavelengths in the network.

To simplify the equations in the later stages, we define function $\Phi(i,j)$ in (2).

$$\Phi(i,j) = \frac{\delta^2}{(\lambda_i-\lambda_j)^2+\delta^2}. \quad (2)$$

Modulator: Due to the imperfection of the coupling mode, a portion of the light is coupled into the ring even when the MR is in the INACTIVE state, which results in a loss in signal power (3).

Regarding a modulator in the ACTIVE state, light will be coupled into the ring, but a portion of the light may pass the modulator, resulting in the modulator's crosstalk. The equation for an ACTIVE state modulator is given in (4). For the general case, the MR is modulating at the resonant wavelength, $\lambda_{MR} = \lambda_j$, where j is the j^{th} wavelength in a waveguide.

$$P_{out}[i] = L_{m_0}P_{in}[i] \ (i = 0..n) \quad (3)$$

$$\begin{cases} P_{out}[j] &= X_{m_1}P_{in}[j] \\ P_{out}[i] &= L_{m_0}P_{in}[i] \quad (i \neq j). \end{cases} \quad (4)$$

Detector: Similar to the modulator, a photo detector is also formed by the MR coupled into a single waveguide. However, different from the modulator, the detector's MR is doped with a Si-Ge layer to detect the incoming optical signal. It needs a converter to convert light into an electrical signal. The detector's models are shown in Fig. 1(c) and 1(d) for the PASSING and DETECTING mode respectively.

When the detector is in the PASSING mode, light from all wavelengths passes the detector, but a portion of the light from all of them is coupled into the ring, resulting in an amount of crosstalk noise being detected at the detector. We define this crosstalk noise as the detector's crosstalk. The output and crosstalk noise is therefore calculated as in (5a) and (5b).

$$P_{out}[i] = L_{d_0}P_{in}[i] (i = 0..n) \quad (5a)$$

$$P_{noise} = X_{d_0}P_{in}[j] + \sum_{i=0}^{n-1}\Phi(i,j)P_{in}[i] \ (i \neq j). \quad (5b)$$

When the detector is in the DETECTING mode, the light signal from the wavelength matching the detector's resonant wavelength is coupled into the detector. The output signal power for the light, which passes the detector, is calculated in (6), while the detected signal power is given in (7). However, some portion of the light from other wavelengths may still be coupled into the ring and detected (8).

$$\begin{cases} P_{out}[j] &= X_{d_1}P_{in}[j] \\ P_{out}[i] &= L_{d_0}P_{in}[i] \quad (i \neq j). \end{cases} \quad (6)$$

$$P_{signal} = L_{d_1}P_{in}[j] \quad (7)$$

$$P_{noise} = \sum_{i=0}^{n-1}\Phi(i,j)P_{in}[i] \ (i \neq j). \quad (8)$$

B. Splitters

Splitters distribute the power from the source to different interconnection paths. Common types of splitters include 1×2 and 1×4 power splitters. The light passes through the splitters and suffers from loss of L_{12} or L_{14}. The equations for 1×2 and 1×4 splitters are thus given in (9) and (10) respectively. For a 1×2 splitter, we consider different split ratios at the two outputs, where output 1 receives $(1-R_{12})$ and output 2 receives R_{12} of the power from the input. For a 1×4 splitter, we consider the same split ratio (i.e. R_{14}) at all the outputs. In this paper, a negligible amount of crosstalk noise introduced by the splitters is considered.

$$P_{out_1} = L_{s_{12}}P_{in}(1-R_{12}) \text{ and } P_{out_2} = L_{s_{12}}P_{in}R_{12} \quad (9)$$

$$P_{out_1} = P_{out_2} = P_{out_3} = P_{out_4} = L_{s14}P_{in}R_{14}. \quad (10)$$

This article has been accepted for publication in a future issue of this journal, but has not been fully edited. Content may change prior to final publication. Citation information: DOI 10.1109/MDAT.2014.2336211, IEEE Design and Test

IV. Corona's Elements Analysis

A. Structure Overview

Corona consists of 256 general-purpose cores grouped into 64 four-core clusters. Three structures are established: optical crossbar for data communication, broadcast bus for multi-casting, and arbitration for protocol. The main laser source is fed into the loop and split into these different structures. For each optical structure, sets of MRs perform as modulators, detectors and injectors. In [2], Table 2 summarizes the Corona optical network's optical elements.

B. Splitter series

In Corona, since only one power waveguide exists, a series of splitters is constructed to split the power from the main source to each processing cluster. Given the analysis of one splitter in Section III, (11) is derived for the power which is split for a particular cluster i. We assume that the split ratio, R_{12}, is fixed for all clusters, and $(1-R_{12})$ is the remaining power source after each cluster. 1×4 splitters are not considered in the splitter series because 1×4 splitters equally distribute the power within the cluster or the channel. Fig. 2(d) shows an example of the splitter series via a hierarchical arrangement in the data channel.

$$P_i = (L_{s_{12}})^i (1-R_{12})^i (L_p)^{d_i} (L_b)^{p_i} (L_{s_{12}})(R_{12})P_{in}$$
$$= (L_{s_{12}})^{i+1} (1-R_{12})^i (L_p)^{d_i} (L_b)^{p_i} (R_{12})P_{in}. \quad (11)$$

In (11), d_i and p_i are respectively the distance and the number of bendings from the power source to the i^{th}-splitter. From (11), we derive that the larger the channel number, the higher the signal loss that the channel suffers due to the fact that it is further from the main laser source.

Calculating d_i, the distance from the source to the i^{th}-splitter

The total die area for Corona is $423mm^2$ (Penryn-based) [2], resulting in $a = 2.05cm$ for each side of the die. For an 8×8 structure, each cluster size is. $\frac{a}{8} = 0.256cm$ We divide these clusters into four 2×8 groups, forming four 16-cluster groups. In each group, the waveguide passes through a two-section L-shape and two 90^o bendings. The first section is a, and the second section is approximated to be two clusters, $\frac{2a}{8} = \frac{a}{4} = 0.513cm$. The distance between two splitters, considering fair distribution, is $d_{splitter} = \frac{a}{16} = 0.128cm$. As a result, (12) expresses the distance travelled from the source to the current splitter.

$$d_i = (i \mod 16)d_{splitter} + (a + \frac{a}{4})\lfloor \frac{i}{16} \rfloor$$
$$= (i \mod 16)d_{splitter} + \frac{5a}{4}\lfloor \frac{i}{16} \rfloor.$$
$$a = 2.05cm$$
$$d_{splitter} = 0.128cm. \quad (12)$$

Calculating p_i, the number of bendings from the source to the i^{th}-splitter

Similar to the previous calculation for d_i, we formulate the number of bendings from the laser source to the current splitter in (13).

$$p_i = 2\lfloor \frac{i}{16} \rfloor. \quad (13)$$

C. Modulators and detectors series

A series of modulators is constructed by cascading the MRs with different resonant wavelengths. In Corona, 64 MRs are cascaded as one series of modulators. When no communication between a cluster X to a cluster Y is set up, the modulators of X are INACTIVE, and the output power is expressed in (14). When communication is set up between X and Y, cluster X's modulators on the communication path of cluster Y are MODULATING. For a long time, all these modulators are in the MODULATING state. The output power after this series of modulators is expressed as (15).

$$P_{out}[i] = (L_{m_0})^n P_{in}[i] \quad (14)$$

$$P_{out}[i] = (L_{m_0})^{n-1} X_{m_1} P_{in}[i]. \quad (15)$$

The detectors are always DETECTING the incoming signal. So we arrive at (16a) and (16b), defining the received output power before each detector j (from 0 to 63) at the wavelength i (from 0 to 63).

$$P_{out_j}[i] = \begin{cases} P_{in}[i] & (\text{j} = 0) \\ (X_{d_1})P_{out_{j-1}}[i] & (\text{j} \neq \text{i and j}-1 = \text{i}) \\ (L_{d_0})P_{out_{j-1}}[i] & (\text{j} \neq \text{i and j}-1 \neq \text{i}) \end{cases} \quad (16a)$$

$$P_{out_j}[i] = \Psi_1(i,j)P_{in}[i] \quad (16b)$$

$$\Psi_1(i,j) = (X_{d_1})^k (L_{d_0})^{j-k}$$
$$\text{k} = 1 \text{ if } \text{j}-1 \geq \text{i}; \text{k} = 0 \text{ otherwise.} \quad (16c)$$

With the defined received power before each detector in (16b), the signal and crosstalk noise power received at each detector j are (17) and (18) respectively.

$$P_{signal_j} = (L_{d_1})P_{out_j}[j] \quad (17)$$

$$P_{noise_j} = \sum_{i=0}^{n-1} \Phi(i,j)P_{out_j}[i] \; (\text{i} \neq \text{j}). \quad (18)$$

V. The Worst-case Crosstalk Noise Analysis For Corona

A. Data Channel

Corona consists of 64 data channels, and each of them is formed by 4 waveguides, 64 wavelengths each. A data channel starts from a cluster called the homecluster, traverses other clusters, where a series of modulators can modulate the light, and finally ends at the homecluster again, with a detectors series and an optical terminator.

This article has been accepted for publication in a future issue of this journal, but has not been fully edited. Content may change prior to final publication. Citation information: DOI 10.1109/MDAT.2014.2336211, IEEE Design and Test

This arrangement results in 64 Multi-Writer-Single-Reader open-ring data-paths, where only one cluster can read from its channel and other clusters only manipulate that channel. Fig. 2 demonstrates the working principle of the optical crossbar.

In Fig. 2, cluster 0's and cluster 63's channels are red and green respectively. Cluster 0's channel (i.e. channel 0) starts from the first splitter and channel 63 is split from the last splitter. All the channels make a loop through the ring before ending at their homeclusters. A communication is set up when other clusters manipulate the light with their modulators series on the homecluster.

In Fig. 2(c), cluster 0 is communicating on channel 63. During the communication, cluster 0's modulators of channel 63 are modulating, while the modulators on the other channels are INACTIVE. Meanwhile, cluster 63's modulators are all INACTIVE, since it does not write to any other clusters. All the detectors of all clusters should be in the DETECTING mode.

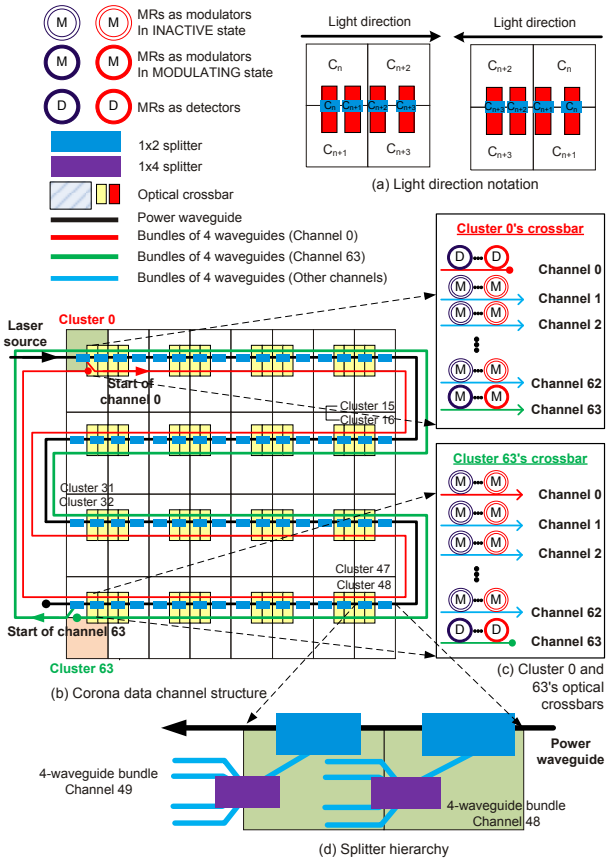

Fig. 2. Data channel overview

With a four-waveguide bundle per data channel, 256 waveguides are required for a complete data path. Hence, a splitter hierarchy consisting of 1×2 and 1×4 splitters is established. Fig. 2(b) shows that the 1×2 splitters are positioned at every channel's beginning to split the source from the power waveguide, and 1×4 splitters are placed after every 1×2 splitter to further divide the power into 4 waveguides.

The study on the splitter series is given in Section IV.B. Instead of P_i, we denote the received power at channel i as P_{data-i}. From (11), the last channel suffers the most signal power loss. Consequently, in the data path, channel 63 suffers the most signal power loss. Fig. 3(a) fully demonstrates a data channel of cluster 63, where cluster 0 desires to communicate with cluster 63. Since every data channel has four waveguides with the same number of detectors and modulators, we can generalize the formula on one waveguide for four waveguides.

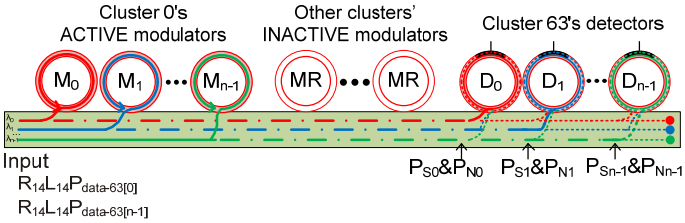

(a) Data channel – Communication between cluster 0 and cluster 63

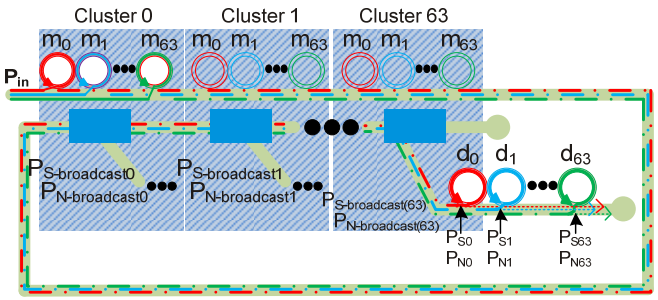

(b) Broadcast bus – Cluster 63 receives a multicast message from cluster 0

Fig. 3. Data channel and broadcast bus

In this case, the signal power and the crosstalk noise received at each detector j are expressed in (19) and (20). P_{S_j} and P_{N_j} are defined in (21a) and (21b) as the signal and the crosstalk noise power received before each detector j of the channel respectively. Also, $\Psi_1(i,j)$ is defined in (16c).

$$P_{signal_j} = (L_{d_1})P_{S_j}[j] \tag{19}$$

$$P_{noise_j} = (L_{d_1})P_{N_j}[j] + \sum_{i=0}^{n-1}\Phi(i,j)(P_{S_j}[i] + P_{N_j}[i])\,(i \neq j) \tag{20}$$

$$P_{S_j}[i] = \alpha_1\Psi_1(i,j)P_{data-N}[i] \tag{21a}$$

$$P_{N_j}[i] = \begin{cases} 0 & (j > i) \\ \alpha_2(L_{d_0})^j P_{data-N}[i] & (j \le i) \end{cases} \tag{21b}$$

where:

$$\alpha_1 = (L_{14})(R_{14})(L_p)^D(L_b)^p(L_{m_0})^{64\times63} \tag{22a}$$

$$\alpha_2 = (L_{14})(R_{14})(L_p)^D(L_b)^p(L_{m_0})^{62\times64+63}. \tag{22b}$$

This article has been accepted for publication in a future issue of this journal, but has not been fully edited. Content may change prior to final publication. Citation information: DOI 10.1109/MDAT.2014.2336211, IEEE Design and Test

B. Broadcast bus

Similar to the data channel, the broadcast bus utilizes modulators and detectors series. However, for multi-casting, the broadcast bus is designated as a single-write multi-read channel. Hence, the differences are the waveguide counts and the splitter hierarchy. Using one waveguide, the broadcast bus starts by a series of modulators from all 64 clusters and arrives at a series of 1×2 splitters, splitting the incoming signal message to all the clusters. A series of 64 detectors at the end of each branch detect and receive the multi-cast message [2]. Fig. 3(b) shows the broadcast bus with notations for the signal power analysis.

In Fig. 3(b), by modulating the light with its series of modulators, cluster 0 multi-casts a message to all other clusters. From Fig. 3(b), the input power for the broadcast bus first suffers loss from all the modulators of the 64 clusters. Similarly, the crosstalk noise from the MODULATING-state modulators also suffers loss from all the other modulators. These loss values are respectively derived in (23a) and (23b), where D is the total distance and N is the total number of bendings for a loop.

$$\alpha_3 = (L_p)^D (L_b)^N (L_{m_0})^{64\times64} \tag{23a}$$

$$\alpha_4 = (L_p)^D (L_b)^N (L_{m_0})^{64\times64-1} (X_{m_1}). \tag{23b}$$

When the signal and crosstalk noise arrive at a cluster x in the broadcast bus, they suffer loss from the splitters series. Propagation and bending loss also accumulate from the first splitter to the x^{th}-splitter. This loss is expressed as (24a) and (24b), where d_x and p_x are the distance and number of bendings from $P_{broadcast}$ to the x^{th}-splitter respectively.

$$\beta_1[x] = (L_{S_{12}})^{x+1} (1-R_{12})^x (R_{12}) (L_p)^{d_x} (L_b)^{p_x} \tag{24a}$$

$$\beta_2[x] = (L_{S_{12}})^{x+1} (1-R_{12})^x (R_{12}) (L_p)^{d_x} (L_b)^{p_x}. \tag{24b}$$

From (23a), (23b), (24a) and (24b), the signal and crosstalk noise power received at cluster x can be expressed in (25) and (26).

$$P_{S-broadcastx}[i] = \alpha_3 \beta_1[x] P_{in}[i] \tag{25}$$

$$P_{N-broadcastx}[i] = \alpha_4 \beta_2[x] P_{in}[i]. \tag{26}$$

At the end of a cluster's channel, a series of detectors detect both the signal and crosstalk noise. From (16a), (16b), (25) and (26), we derive (27) and (28), where $\Psi_1(i,j)$ is defined in (16c).

$$P_{S_j}[i] = \Psi_3(i,j) P_{S-broadcast(x)}[i] \tag{27}$$

$$P_{N_j}[i] = \begin{cases} 0 & (j > i) \\ (L_{d_0})^j P_{N-broadcast(x)}[i] & (j \le i) \end{cases}. \tag{28}$$

Further investigating the signal power and crosstalk noise received at each detector, we derive (29) and (30) for the signal and crosstalk noise received at each detector j in the broadcast bus of cluster 63.

$$P_{signal_j} = (L_{d_1}) P_{S_j}[j] \tag{29}$$

$$P_{noise_j} = (L_{d_1}) P_{N_j}[j] + \sum_{i=0}^{n-1} \Phi(i,j)(P_{S_j}[i] + P_{N_j}[i]). \tag{30}$$

VI. Result and Discussion

Utilizing the analytical models with the values for the listed parameters, we calculate the crosstalk noise and SNR received at each detector of cluster 63. (19), (20), (29) and (30) respectively represent the signal power and crosstalk noise received at each detector of the data channel and broadcast bus. The SNR is expressed by (31).

$$SNR = \frac{P_{signal}}{P_{noise}}. \tag{31}$$

The SNR is defined as the ratio between the received signal and the crosstalk noise power at the detectors. When substituting (19), (20) or (29), (30) into (31), the input power for the signal power in the numerator P_{signal} and that for the crosstalk noise power in the denominator P_{noise} cancel out each other. Hence, the SNR is independent of the input signal power of the network.

Regarding the data channel, the worst-case power loss is -69.3dB at the last detector. The worst-case SNR is 14.0dB at the 43rd detector, where the signal power loss is -69.2dB. On the broadcast bus, the signal and crosstalk noise at each cluster in the broadcast bus differ in the number of splitters. Following the analysis of the splitter series in Section IV.B, the last splitter has the highest power loss. As a result, we calculate the SNR values of cluster 63. Similar to the data channel, the worst-case SNR is 14.0dB at the 43rd detector; the worst-case power loss is 63.4dB at the 63rd detector. Since the broadcast bus does not contain 1×4 splitters, its worst-case signal and crosstalk noise power loss are both smaller compared to those of the data channel.

Fig. 3 demonstrates the values of the signal power loss, crosstalk noise power loss and SNR at different detectors of the data channel and the broadcast bus. According to our analytical model, both signal and crosstalk noise suffer from propagation, bending and passing loss. This reflects the downtrend of both the signal power loss and crosstalk noise power loss in Fig. 3. However, the results also show that the crosstalk noise power reduces more deeply compared to the signal power. On the one hand, at first, the crosstalk noise power slightly decreases due to the decreasing number of optical signals on different wavelengths that introduce crosstalk noise. Toward the last detectors (i.e. the 60^{th}-detector onwards), when only a small number of optical signals contribute to the noise, this crosstalk noise decreases deeply. On the other hand, the signal power decreases more steadily when the detectors' number increases. Consequently, the worst-case SNR slightly decreases among the first detectors, reaches its minimum at detector 43, starts to increase and finally peaks at the last detector.

From our analyses, the Q-factor can substantially affect the SNR. Fig. 3 shows the destructive impact of Q. Indeed, the SNR is even negative when Q is smaller than 2000. For example, when Q=100, the worst-case SNR is -11.5dB. A small Q-factor corresponds to the drop port and is different from that of the through port. When Q-factor is fairly small, the crosstalk power exceeds the signal power

This article has been accepted for publication in a future issue of this journal, but has not been fully edited. Content may change prior to final publication. Citation information: DOI 10.1109/MDAT.2014.2336211, IEEE Design and Test

received at the detectors. Additionally, from Fig. 3, the SNR tends to gradually settle at a value toward a higher Q-factor. Thus, a Q-factor larger than 15,000 may not significantly improve the SNR.

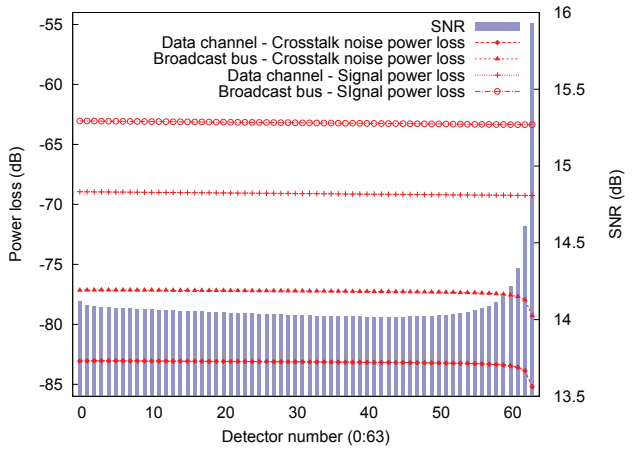

(a) Power loss, crosstalk noise and SNR at different detectors (Q=9,000)

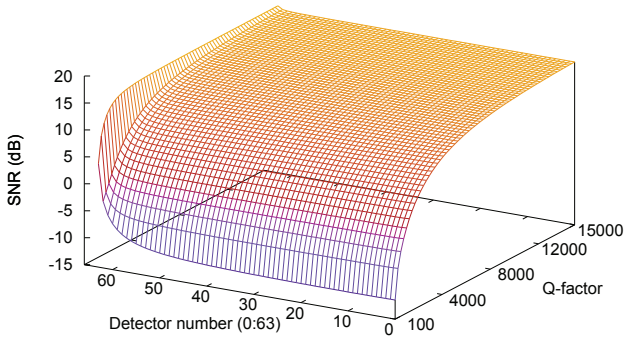

(b) The worst-case SNR with different Q-factors

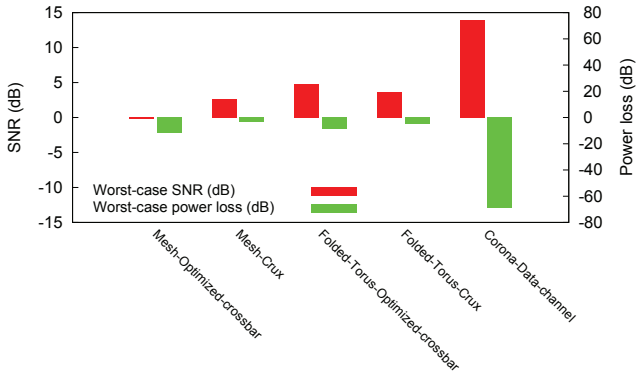

(c) Comparison of the worst-case SNR and signal power loss

Fig. 4. The signal and crosstalk noise power loss and worst-case SNR in Corona; and the comparison to Mesh and Folded-torus ONoCs

Furthermore, since 64 clusters of Corona are arranged in an 8×8 matrix, we can consider counterpart mesh-based and folded-torus-based ONoCs with a similar clusters' matrix-size. Hence, comparison of the worst-case SNR and signal power loss is performed for the three ONoCs. The results in the mesh and folded-torus are quantitatively simulated in CLAP, an automated Crosstalk and Loss Analysis Platform. CLAP can perform the analyses of crosstalk noise, signal power loss and SNR of single-wavelength-ONoCs using an arbitrary optical router [5]. MATLAB is utilized to simulate Corona's results.

Fig. 3 shows the comparison among the three ONoCs. The comparison results indicate that the worst-case SNR in Corona is better than that of the mesh-based and folded-torus-based ONoCs. Corona's worst-case SNR is 14.0dB, compared to -0.2dB and 3.6dB in the mesh-based using the Optimized-Crossbar router and the folded-torus-based using the Crux optical router respectively [5]. However, Corona's worst-case power loss is substantially higher, -69.3dB, compared to -11.9dB and -9dB in the mesh-based and folded-torus-based ONoCs respectively.

VII. Conclusion

Crosstalk noise is an inevitable characteristic of microresonator-based switches used in constructing ONoCs. At the network level, crosstalk noise accumulates and considerably damages the SNR and scalability of ONoCs. Indeed, the worst-case crosstalk noise and SNR analyses in a specific ONoC are profoundly dependent on the specific architectural properties of that network. This paper focuses on the analyses of crosstalk noise in two structures of the Corona. However, at the device level, our developed analytical models can be utilized in any other topology using WDM. Utilizing the proposed analytical method, quantitative simulations of the worst-case power loss, crosstalk noise and SNR in Corona are achieved. Results indicate that the worst-case SNR in the data network of Corona is 14.0dB, while the worst-case power loss is significantly high: -69.3dB. Additionally, we compare thee worst-case SNR, power loss and crosstalk noise in Corona with those in mesh-based and folded-torus-based ONoCs of the same network size. The comparison shows that Corona's worst-case power loss is substantially higher, although it has better worst-case SNR.

References

[1] J. Xu, W. Wolf, *et al.*, "A methodology for design, modeling, and analysis of networks-on-chip," *IEEE International Symposium on Circuits and Systems (ISCAS)*, vol.2, pp. 1778–1781, May 2005.

[2] D. Vantrease, R. Schreiber *et al.*, "Corona: System implications of emerging nanophotonic technology," in *35th International Symposium on Computer Architecture*, 2008, pp. 153–164.

[3] R. W. Morris and A. K. Kodi, "Design of on-chip networks using microring-resonator based nanophotonic crossbar for future multicores," in *23rd Annual Meeting of the IEEE Photonics Society*, 2010, pp. 558–559.

[4] J. Ahn, M. Fiorentino *et al.*, "Devices and architectures for photonic chip-scale integration," *Applied Physics A*, vol. 95, no. 4, pp. 989–997, 2009.

[5] M. Nikdast, J. Xu *et al.*, "Systematic analysis of crosstalk noise in folded-torus-based optical networks-on-chip," *IEEE Transactions on Computer-Aided Design of Integrated Circuits and Systems*, vol. 33, no. 3, pp. 437–450, Mar 2014.

[6] C. H. Chen, "Waveguide crossings by use of mutlimode

This article has been accepted for publication in a future issue of this journal, but has not been fully edited. Content may change prior to final publication. Citation information: DOI 10.1109/MDAT.2014.2336211, IEEE Design and Test

tapered structures," in *21st Annual Wireless and Optical Communications Conference (WOCC)*, 2012, pp. 130–131.

[7] Q. Xu, B. Schmidt et al., "Cascaded silicon micro-ring modulators for wdm optical interconnection," *Opt. Express*, vol. 14, no. 20, pp. 9431–9435, Oct 2006.

[8] S. Xiao, M. H. Khan *et al.*, "Modeling and measurement of losses in silicon-on-insulator resonators and bends," *Opt. Express*, vol. 15, no. 17, pp. 10 553–10 561, 2007.

[9] P. Dong, W. Qian *et al.*, "Low loss silicon waveguides for application of optical interconnects," in *IEEE Photonics Society Summer Topical Meeting Series*, 2010, pp. 191–192.

[10] F. Xia, M. Rooks *et al.*, "Ultra-compact high order ring resonator filters using submicron silicon photonic wires for on-chip optical interconnects," *Opt. Express*, vol. 15, no. 19, pp. 11 934–11 941, 2007.

[11] A. Joshi, C. Batten *et al.*, "Silicon-photonic clos networks for global on-chip communication," in *3rd ACM/IEEE International Symposium on Networks-on-Chip*, 2009, pp. 124–133.

[12] A. Biberman, B. Lee *et al.*, "Demonstration of all-optical multiwavelength message routing for silicon photonic networks," in *Conference on Optical Fiber communication/National Fiber Optic Engineers Conference*, Feb 2008, pp. 1–3.

Luan H.K. Duong (S'14) received the B.S. degree in Computer Science from The Hong Kong University of Science and Technology (HKUST) in 2012. He is currently working towards the Ph.D. degree in Electronic and Computer Engineering at HKUST. His research interests include embedded system, systems-on-chip and optical networks-on-chip.

Mahdi Nikdast (S'10-M'14) received his Ph.D. degree in Electronic and Computer Engineering from The Hong Kong University of Science and Technology in 2013. He is currently a visiting scholar in the Mobile Computing System Laboratory at HKUST. His research interests include embedded and computing systems, multiprocessor systems-on-chip, networks-on-chip, and optical interconnection networks.

Sébastien Le Beux (IEEE Member) is Associate Professor at Ecole Centrale de Lyon since 2010. In 2007, he obtained a PhD from the University of Lille. He has authored or co-authored over 40 book chapters, journal publications and conference papers. His research interests include design methods for emerging (nano)technologies and embedded systems.

Jiang Xu (S'02-M'07) received his Ph.D. degree from Princeton University in 2007. He is an Associate Professor at Hong Kong University of Science and Technology. He authored and coauthored more than 70 book chapters and papers in peer-reviewed journals and international conferences. His research areas include embedded system, optical interconnects and HW/SW codesign.

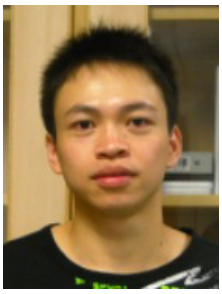

Xiaowen Wu (S'12) received BSc degree in computer science from the Harbin Institute of Technology, China in 2008. He is currently working towards the Ph.D. degree in Electronic and Computer Engineering at the Hong Kong University of Science and Technology. His research interests include embedded systems, multiprocessor systems, and networks-on-chip.

Zhehui Wang received B.S. degree in electrical engineering from Fudan University, China in 2010. He is currently working towards the Ph.D. degree in Electronic and Computer Engineering at the Hong Kong University of Science and Technology. His research interests include embedded system, multiprocessor systems, and floorplan design for network-on-chip.